Int. J. Nanosci. Nanotechnol., Vol. 20, No. 4, Dec. 2024, pp. 295-304
DOI: https://doi.org/10.22034/ijnn.2025.2025216.2493

Investigation of Structural, Dielectric, and Magnetic Properties of $ZnFe_2O_4$ Prepared by Single-Step Chemical Route Method

R. Ramesh[1*], D. Lakshmi[1], and K. Kaviyarasu[2]

[1]Department of Physics, Sacred Heart College (Autonomous), Tirupattur- 635601 (Affiliated to Thiruvalluvar University), Tamil Nadu, India
[2]UNESCO-UNISA Africa Chair in Nanosciences/Nanotechnology Laboratories, College of Graduate Studies, University of South Africa (UNISA), Muckleneuk Ridge, PO Box 392, Pretoria, South Africa

(*) Corresponding author: rramesh@shctpt.edu
(Received: 19 March 2024 and Accepted: 10 October 2024)

Abstract

In this study, we have successfully synthesized $ZnFe_2O_4$ nanoparticles by the one-step chemical route method. The structure of the sample was identified as a tetragonal phase by the X-ray diffraction (XRD) studies. Scanning electron microscopy (SEM) analysis showed the uniform spherical distribution of the particles with the range of 20 nm to 60 nm. The formation of metal–oxygen bonds (Zn–O and Fe–O) was confirmed by absorption bands observed at 531 cm^{-1} and 497 cm^{-1} in the Fourier transform infrared (FTIR)spectrum. The optical bandgap of the synthesized $ZnFe_2O_4$ nanoparticles was estimated from the Tauc plot as 5.37 eV based on the absorption spectrum resulting from UV-vis studies. Electrical performance including dielectric loss, dielectric constant, and permittivity, of the prepared Zinc ferrite nanoparticles were studied and the behavior of the sample at various temperatures was plotted and interpreted.

Keywords: *Zinc ferrite, chemical route, dielectric measurement, Electron microscopy, magnetic behavior*

1. INTRODUCTION

The production of nanomaterials and various nanostructures is of great interest because of its shell effect. Metal oxides like ZnO, FeO, NiO, MnO, etc., have limited applications because of their narrow optical bandgap and magnetic properties [1-5]. WO_{3-x} doped $ZnFe_2O_4$ semiconductor prepared by the combined method of hydrothermal and calcination methods showed a good Photon-Fenton activity due to the effective charge transmission and the faster LVX degradation [6]. If these metal oxides were combined utilizing any physical or chemical methods, they could be converted as a suitable material for numerous applications. Various factors like temperature, pH, synthesis method, and calcination temperature modify the physical and chemical properties of nanomaterials and nanocomposites [7-9]. Recently researchers have been concentrating on the preparation of metal ferrites because of their enhanced magnetic properties and their applications in many fields. Many ferrites including zinc ferrite, nickel ferrite, manganese doped zinc, and nickel ferrites found to have superparamagnetic behaviors and due to this reason, they find applications in devices like cores of the transformers, inductor-based devices, microwave devices, radars, antenna rods, etc., Nanocomposites of polypyrrole (PPY)-supported steps scheme (S-Scheme) $ZnFe_2O_4$@WO_{3-x} (PZFW15) prepared by multistep process formed the heterojunction which promotes and increases the redox power in the presence of the electric field [10].

There are numerous methods exist for the preparation of the zinc and nickel ferrites

including thermal treatment, ball milling technique, chemical route, green synthesis, solvothermal, etc [11-14]. All these methods of preparation have their effect on the preparation process which controls the size of the particles, it may affect the morphology, change the optical behavior, and affect the magnetic properties. A study reported on the preparation of zinc ferrite by the co-precipitation method possessed very low coercivity and the particle size was about 4.5 nm to 15 nm [15-17]. Hydrothermally synthesized B-rGO/$ZnFe_2O_4$ photocatalyst served as a worthy photocatalytic system for water splitting by the band mechanism of BrGO nanosheets and ZnF nanoparticles upturned the V-shaped Mott-Schottky plots with 100% best activity and hydrogen production [18]. An effective and economically feasible magnetic-based semiconductor PANI-sensitized g-C_3N_4/$ZnFe_2O_4$ photocatalyst showed a good result in the removal of toxic compounds like Cr (VI) and phenol from the wastewater for environmental remediation was reported [19].

Ferrites are found to have very high resistivity and thus help in the prevention of the production of eddy currents in the applied alternating magnetic field and because of this property ferrites are found to have a few applications in high-frequency devices. One of the recent studies reported on the green synthesis of zinc ferrite by using the seed extract of *Piper nigrum* which had a particle size in the range of 60 nm to 80 nm [20-21]. Several reports have established the photocatalytic activity of the zinc ferrites, among other ferrites, it found to have better photocatalytic activity in the degradation of selected dyes. For instance, a recent study on the preparation of zinc ferrite by ball milling ZnO and α-Fe_2O_3 in the 1:1 molar ratio posed high photocatalytic activity on methylene blue [3, 21]. Nowadays alloys and permalloys were found to be the better replacement for corrosive iron and steel materials. A combination of nickel and zinc doped ferrites was behaving as alloys in designing hard components of many industrial pieces of machinery. For instance, a study reported on the preparation of Ni/Zn-ferrite permalloy by the electro-infiltration process was investigated and found to have strong bonding of metal ions of Ni and Zn [22, 23]. Ferrites can be used to produce micro compounds with a property of single negative (SNG) metamaterial, A recent study on the synthesis of Mg-doped zinc ferrite base flexible material by the sol-gel method was reported [24, 25]. Zinc ferrites were found to have good application in the field of medicine. A recent study on the zinc ferrite prepared by the co-precipitation method was analyzed for its antimicrobial, wound healing promoting activity, and for the dermatological applications was tested, its cyto compatibility and hemo compatibility were tested and found that zinc ferrite can be used as a drug curing the wounds and other related disorders [26,60].

In this investigation, we account for the single-step chemical route production of zinc ferrite by using zinc nitrate hexahydrate and iron oxide without using any reducing or capping agents. The single-step chemical route has some advantages which involve a rapid reaction mechanism, no need to use any precipitating agents, and reducing agents, precursors, and dopant itself act as donors and acceptors in the formation of nanoparticles [27, 28]. It also prevents the production of too many impurities during the process of synthesis. Here in this study, the synthesized zinc ferrite sample was characterized for its structural, optical, morphological, and dielectric properties.

2. EXPERIMENTAL SECTION

2.1. Materials and Method

In this study, the precursor material is zinc nitrate hexahydrate, and Fe-O is dissolved in sulfuric acid as the dopant material. All the chemicals were of pure AR grade and utilized in this experimental study with no further purification. The method adopted in this study is a direct one-step chemical

[9,12,62] route method in which the precursor material solution was prepared, and iron oxide was mixed in 1mole ratio to initiate the reaction mechanism

2.2. Synthesis of $ZnFe_2O_4$ Nanoparticles

Zinc ferrite NPs by direct one-step chemical route method by dissolving 18.936 g/mol of $[Zn(NO_3)_2.6H_2O]$in water and 15.969 g/mol of Fe-O in sulphuric acid and stirred well in the magnetic stirrer for 6 h in the laboratory at room temperature with pH level 10 as per the reported literature. After vigorous stirring of the solution, a dark brown color precipitate was obtained [13, 14]. The solution mixture was centrifuged at 10000 rpm and the sediment was dried at 180 °C for 4 h in a hot air oven to remove residual impurities. The dried powder was calcined in the furnace for 4 h at 800 ºC to remove the nitrites and the final product obtained was kept airtight in a container for further investigation.

3. RESULTS AND DISCUSSION

3.1. Powder X-ray Diffraction

In this investigation, the prepared zinc ferrite NPs were analyzed for their structural information by the Perkin Elmer instrument in the 2θ range 20º to 70º. The recorded spectrum was indexed, and the strong peaks observed in the planes with (hkl) values (112), (213), (004), (412), (423), (442), (603), and (543) were correctly correlated utilizing the available standard records (JCPDS, card no: 48-0567) and the crystalline arrangement was recognized to be a tetragonal phase [15]. The grain dimension of the synthesized sample was calculated using Debye's Scherer's formula and the estimated particle size of 28 nm. The XRD pattern of $ZnFe_2O_4$ as shown in Fig. 1.

3.2. FTIR Spectroscopic Analysis

The prepared $ZnFe_2O_4$ nanoparticles were examined using FTIR spectroscopy to find the molecular bonding and the functional groups present in the sample. The spectra were recorded with % of transmittance versus wavenumber (cm^{-1}) between the range 200 cm^{-1} to 2000 cm^{-1}.

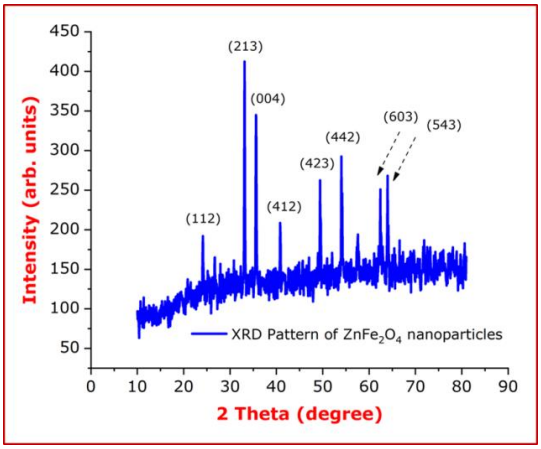

Figure 1. *XRD Pattern of $ZnFe_2O_4$ nanoparticles*

The recorded FTIR spectrum of zinc ferrite is shown in Fig. 2. The absorption peaks obtained at specific frequencies in the fingerprint region 497 cm^{-1} confirm the formation of bonding between Zn and Fe-O sites, which is due to the vibrations produced in the A site of the tetrahedral band and B sites of the octahedral band of the ferrite compound [16, 17,63]. Also in this investigation, the absence of the peaks in the range of 1000 cm^{-1} - 1300 cm^{-1} and above 3000 cm^{-1} confirms the absence of C-O, O-H, and C=H bonds of organic substances and hence the purity is maintained in the process [18]. The calcination temperature played a vital role in the removal of unwanted ions that may contaminate the reaction during the preparation of the zinc ferrite.

3.3. UV-Visible Spectroscopic Studies

UV-visible spectral graph and *Tauc plot* of the prepared zinc ferrite nanoparticles by chemical route method are given in Fig. 3(a-b). The spectrum was analyzed within the optical window region from 200 nm to 700 nm. The term '*energy gap'* is mentioned as the difference of energy between the valence band (VB) to the conduction band (CB) and electrons are jumped from one band to another band that is electrons are

jumped from the outermost band to the conduction band [18]. The spectrum was

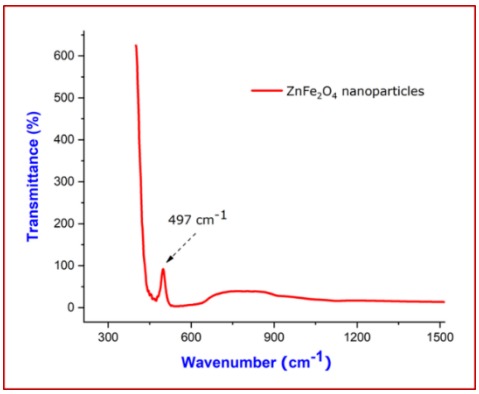

Figure 2. *FTIR spectrum of $ZnFe_2O_4$ nanoparticles*

analyzed within the optical window region from 200 nm to 700 nm. The term '*energy gap'* is mentioned as the difference of energy between the valence band (VB) to the conduction band (CB) and electrons are jumped from one band to another band that is electrons are jumped from the outermost band to the conduction band [18]. The highest photocatalytic activity due to tunable band structure synergetic effect of broad absorption in the NIR region was done by ZFCN@20PPY composites [28]. Highly effective Photo-Fenton degradation of phenol and chromium (Cr-VI) under sunlight with the modified Al_2O_3 MCM-41 $ZnFe_2O_4$ showed an appreciable band edge potential of hydroxyl radical generation [29]. In general, the deviation in the particle size results in the blue shift of the bandgap and it can be due to the quantum size effect and due to the creation of defect centres produced by the doping materials in the local lattice. Here a strong absorption peak at 242 nm was found and by using the cut-off wavelength 201.64 nm the energy gap E_g of the zinc ferrite nanoparticles was plotted and found as 5.37 eV [19, 20] by using the general formula:

$$E_g = hc/\lambda \quad (1)$$

3.4. Morphological Analysis

The morphological nature of the synthesized NPs was analyzed with SEM instrumentation and the typical recorded SEM image of the synthesized $ZnFe_2O_4$ nanoparticles as shown in Fig. 4(a-d). It

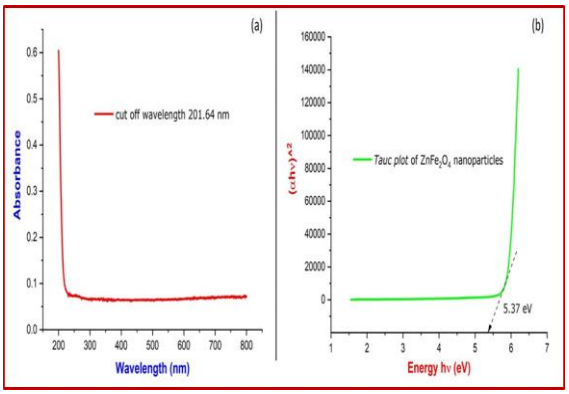

Figure 3. *(a) UV-visible spectrum and (b)Tauc plot of $ZnFe_2O_4$*

depicts that the sample contains a micron-scale aggregation of small uniformly distributed spherical particles [21, 22]. The existence of highly dense agglomeration and the homogeneous shape of particles indicates the pore-free crystalline surface nature of the synthesized specimen. It showed a closely packed spheroid of more or less uniform-sized structures with an average size of 20 nm to 60 nm and agrees with the recorded XRD structure [63].

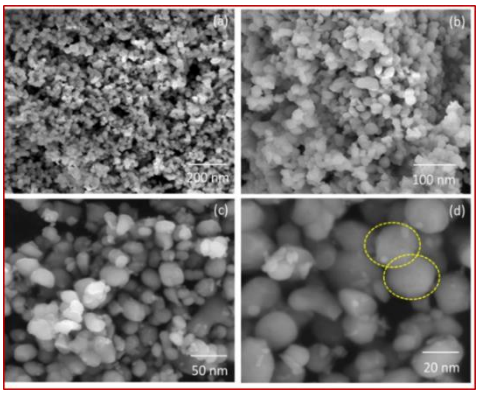

Figure 4(a-d). *SEM Images of $ZnFe_2O_4$* nanoparticles.

3.5. Electrical Performance of $ZnFe_2O_4$

3.5.1. Complex Impedance Analysis

The $ZnFe_2O_4$ NPs were pressed into pellets and were studied at various temperature ranges from 50 ºC to 250 ºC and the variation of impedance with frequency was plotted. From the result, for the real part of the impedance, it was observed the

impedance was found to be value maximum for the applied alternating current in the low-frequency band and started in the low region and started decreasing exponentially while increasing the frequency and it remains constant at high temperature [23, 29]. A similar trend is followed for the case imaginary part also. Fig. 5(a-b) illustrates the frequency and temperature reliance of the impedance. At the same time, the complex impedance graph called as Nyquist plot was plotted as shown in Fig. 6. It was noted that an overlapping semicircle is obtained in the low-frequency region at high temperatures, whereas a smaller diameter curve was obtained for the medium temperature level (150 ºC and 200 ºC) which depicts the electrode - dielectric material interface contribution due to grain boundary and high conductivity [25, 30, 31].

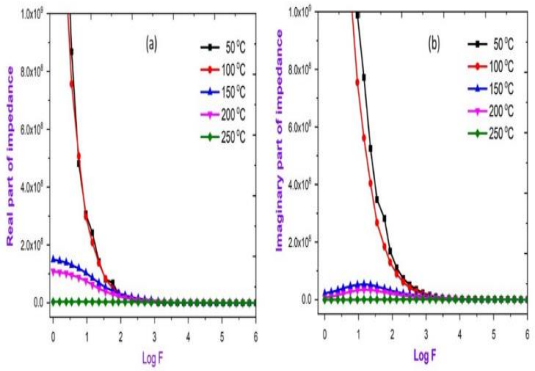

Figure 5(a-b). *The real part of the impedance and imaginary part of the impedance of $ZnFe_2O_4$ nanoparticles.*

3.5.2. Permittivity

Permittivity is described as a thermodynamic function that relies upon the frequency of the applied electric field. The real component and the imaginary component of the permittivity of the $ZnFe_2O_4$ sample were examined with different temperature ranges as shown in Fig. 7(a-b). From the result, it was observed that the permittivity was maximum at low frequency for all the temperature ranges (150 ºC, 200 ºC & 250 ºC) and started decreasing in the mid-frequency level and attained a constant value which is independent of frequency and temperature was observed in the case of the real and imaginary part [26]. This may be due to charge migration and electric dipole reorientation, the distribution varies with temperature [27, 28]. At low frequencies it

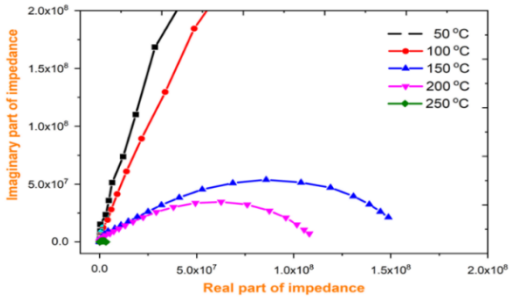

Figure 6. *Nyquist plot of $ZnFe_2O_4$*

is due to ionic relaxation, at the medium frequency it is due to dipolar relaxation, and at high frequencies, it is due to atomic and electronic resonances which are produced from the vibrations, rotations of ions, or electrons. Some of the ions of zinc may get evaporated at very high temperatures and create a small distortion in the lattice plane of the crystal and it accelerates the hopping mechanism between the Fe ions in the +2 oxidation states and hence increases the polarization effect inducing the charge carriers to accumulate in the grain boundaries of the sites [29].

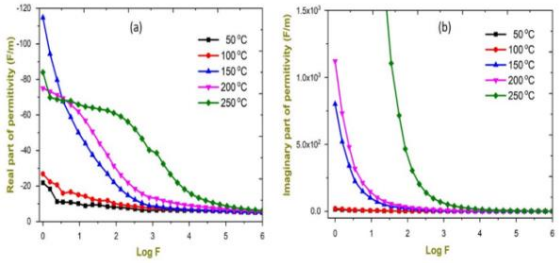

Figure 7(a-b). *The real and imaginary part of permittivity of $ZnFe_2O_4$ nanoparticles.*

3.5.3. Conductivity and Resistivity Measurement of the Sample

The conductivity of the sample was measured at various temperatures ranging from 50 ºC to 250 ºC with the applied frequency shown in Fig. 8(a-b). Conductivity in the material takes place

because of the migration of the ions when it is encountered by the externally applied field which activates the carriers. Several studies reported on the performance of nickel-doped cadmium and other ferrite materials based on the effect produced by the ferrous ions in the exchanging mechanism of interactions [30-33]. From the result, it was noted that the sample possesses high conductivity at high temperatures in the entire frequency range. The sample's conductivity is minimum at the lower frequency domain and started increasing gradually with the high-frequency domain implying the frequency dependence of the grain boundaries. The changes observed in the AC conductivity concerning frequency are attributed to the reason of the electrical energy of the a.c electric field and thus the release of the trapped charges generates the relocation of ions connecting the limited states. The resistivity of the sample was studied in the temperature range of 50 ºC to 250 ºC with frequency. Results showed that the Resistivity decreased drastically with increasing temperature and approached very low values at (250 ºC) in the entire frequency range. For medium temperatures (200 ºC and 150 ºC) it was quite high in the low frequency and gradually decreased while increasing the frequency and almost becoming frequency independent. At low temperatures (50 ºC and 100 ºC) the samples possess high resistivity and approached a low value with rising frequency, and this is due to the immobility of the charge carriers [34].

3.5.4. Dielectric Constant and Dielectric Loss

The plot of frequency dependence of the dielectric constant with various temperature ranges is given in Fig. 9(a-b). The dielectric constant value is maximum in the low-frequency region for the samples at high temperatures (150 ºC, 200 ºC, and 250 ºC) and then decreases with increasing frequencies. At low frequencies, it is due to the contribution of multicomponent polarization [35]. At high frequencies, it

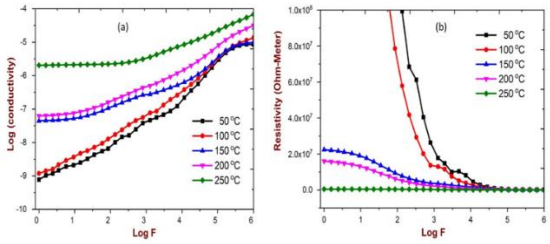

Figure 8(a-b). *Variation of conductivity and resistivity with frequency of $ZnFe_2O$ nanoparticles.*

approaches constant values with increasing frequencies attributed to only the interfacial polarization [36]. This change in dielectric constant is due to the space charge polarization created by the higher conductivity phases in the boundaries of the dielectric material [37-39]. When the frequency is increased, the dipoles may not tag on the speedy deviation of the functional a.c field and thus there is a decrease in the polarization that distorts electrons of the ferrite material [40- 46]. It can be attributed to the dipoles attaining rotational freedom and affecting molecular interaction energy which becomes weaker. A similar trend is followed in both the case of a dielectric loss with frequency [47-50].

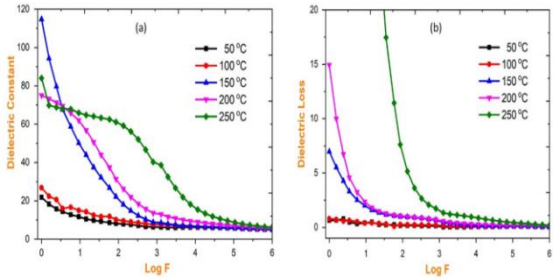

Figure 9(a-b). *Dielectric constant and dielectric loss of $ZnFe_2O_4$ nanoparticles.*

3.6. VSM Studies of $ZnFe_2O_4$

The magnetic property of the synthesized $ZnFe_2O_4$ nanoparticles were studied VSM analytical instrument at room temperature as shown in Fig. 10. From the result of the *M-H hysteresis curve*, it was observed that the width or the area of the curve is almost negligible, and it appeared as *S*-shaped [50-

54]. According to many reports the zinc ferrites have a superparamagnetic property with very low coercivity values [55-59]. It is observed that zinc ferrite exhibits a hysteresis curve with nearly negligible remanence and coercivity which depicts the unique property of superparamagnetic, saturation magnetization (M_s), and coercivity (H_c) of the samples were calculated as 1.72 emu/g and 0.0004 emu/g, which is almost negligible and similar behavior were reported in literature for the soft ferrite materials and it is attributed to the reason that the degree of inversion is greater for the smaller sizes particles [60-63].

4. CONCLUSION

In conclusion, we report that $ZnFe_2O_4$ nanoparticles were successfully synthesized by the chemical route method. The structural arrangement of the synthesized sample was identified as a tetragonal phase using the XRD studies. The bonding arrangement of the Zn and Fe-O has been established from the observed peaks 497 cm^{-1} using FTIR spectroscopy. The uniform spherical distribution of the nanomaterial surface morphology was analyzed using SEM and the average size was estimated to be 20 nm to 60 nm. The optical bandgap of the synthesized $ZnFe_2O_4$ nanoparticles was calculated as 5.37 eV using the *Tauc plot*.

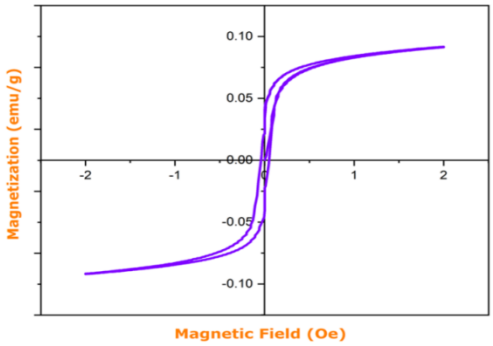

Figure 10. *VSM studies of $ZnFe_2O_4$ nanoparticles.*

Dielectric studies were performed at various temperatures with frequency, including impedance analysis, dielectric loss, dielectric constant, permittivity, conductivity, and resistivity respectively. VSM studies confirmed the superparamagnetic nature of the sample.

CONFLICT OF INTEREST

The authors declare that they have no conflict of interest.

REFERENCES

1. Harikrishnan, R., Mani, G., Mani, M., Kaviyarasu, K., Baskaran, I., "One step microwave assisted synthesis of praseodymium orthoferrite nanoparticles: Rietveld refinement phase matching, optical, and magnetic property analysis", *Physica B: Condensed Matter,* 639 (2022) 414019.
2. Magdalane, C. M., Priyadharsini, G. M. A., Kaviyarasu, K., Jothi, A. I., Simiyon, G. G., "Synthesis and characterization of TiO2 doped cobalt ferrite nanoparticles via microwave method: Investigation of photocatalytic performance of congo red degradation dye", *Surfaces and Interfaces*, 25 (2021) 101296.
3. Kombaiah, K., Vijaya, J., Kennedy, L., Bououdina, M., Kaviyarasu, K., Ramalingam, R., Murugan, A., Bulla, A., "Effect of Cd 2+ concentration on ZnFe 2 O 4 nanoparticles on the structural, optical and magnetic properties", *Optik - International Journal for Light and Electron Optics*, 135 (2017) 190-199.
4. Slavu, L. M., Rinaldi, R., Di-Corato, R., "Application in Nanomedicine of Manganese-Zinc Ferrite Nanoparticles", *Appl. Sci.,* 11 (2021) 11183.
5. Zhang, Y., Kohler, N., Zhang, M. Q., "Surface modification of superparamagnetic magnetite nanoparticles and their intracellularuptake", *Biomaterials,* 23 (2002) 1553–1561.
6. Kumar-Das, K., Mansingh, S., Prava-Sahoo, D., Mohanty, R., Parida, K., "Engineering Oxygen vacancy mediated Step-scheme charge carrier dynamic coupling WO3-X/ZnFe2O4 heterojunction towards robust photo-Fenton driven Levofloxacin detoxification", *New Journal of Chemistry*, 46(12) (2022) 5785-5798.
7. Dadfar, S. M., Roemhild, K, Drude, N. I., Von-Stillfried, S., Knuchel, R. Kiessling, F., Lammers, T., "Iron oxide, nanoparticles: Diagnostic, therapeutic and theranostic applications", *Adv. Drug Deliv. Rev.,* 138 (2019) 302-325.
8. Doaga, A., Cojocariu, A. M., Amin, W., Heib, F., Bender, P., Hempelmann, R., Caltun, O. F., "Synthesis and characterizations of manganese ferrites for hyperthermia applications", *Mater. Chem. Phys.,* 143 (2013) 305-310.

9. Thakur, P., Chahar, D., Taneja, S., Bhalla, N., Thakur, A., "A review on MnZn ferrites: Synthesis, characterization and applications", *Ceram. Int.,* 46 (2020) 15740-15763.
10. Kumar Das, K., Prava Sahoo, D., Mansingh, S., Parida, K., "$ZnFe_2O_4$@WO_{3-x}/Polypyrole: An efficient ternary photocatalytic system for energy and environmental application", *ACS Omega*, 45(6) (2021) 30401-30418.
11. Kareem, S. H., Ati, A. A., Shamsuddin, M., Lee, S. L., "Nanostructural, morphological and magnetic studies of $PEG/Mn_{(1-X)}Zn_xFe_2O_4$ nanoparticles synthesized by co-precipitation", *Ceram. Int.,* 41 (2015) 11702-11709.
12. Salehpour, F., Khorramdin, A., Shokrollahi, H., Pezeshki, A., Mirzaei, F., Nader, N. D., "Synthesis of Zn-doped manganese ferrite nanoparticles via coprecipitation method for magnetic resonance imaging contrast agent", *J. Nanotechnol. Eng. Med.,* 5 (2014**)** 041002.
13. Arulmurugan, R., Jeyadevan, B., Vaidyanathan, G., Sendhilnathan, S., "Effect of zinc substitution on Co–Zn and Mn–Zn ferrite nanoparticles prepared by co-precipitation", *J. Magn. Magn. Mater.,* 288 (2004) 470-477.
14. Hejase, H., Hayek, S. S., Qadri, S., Haik, Y., "MnZnFe nanoparticles for self-controlled magnetic hyperthermia", *J. Magn. Magn. Mater.,* 324 (2012**)** 3620-3628.
15. Zeng, H., Rice, P. M., Wang, S. X., Sun, S., "Shape-Controlled synthesis and shape-induced texture of MnFe2O4 nanoparticles`*J. Am. Chem. Soc.,* 126 (2004**)** 11458-11459.
16. Orsini, N. J., Milic, M. M., Torres, T. E., "Zn- and (Mn, Zn)-substituted versus unsubstituted magnetite nanoparticles: Structural, magnetic and hyperthermic properties", *Nanotechnology,* 31 (2020) 225707.
17. Makovec, D., Kodre, A., Arˇcon, I., Drofenik, M., "Structure of manganese zinc ferrite spinel nanoparticles prepared with coprecipitation in reversed microemulsions", *J. Nanoparticle Res.,* 11 **(**2008**)** 1145-1158.
18. Das, K. K., Paramanik, L., Parida, K., "An insight to band-bending mechanism of polypyrrole sensitized B-rGO/ZnFe2O4 p-n heterostructure with dynamic charge transfer for photocatalytic applications", *International Journal of Hydrogen Energy*, 46(48) (2021) 24484-24500.
19. Patnaik, S., Das, K. K., Mohanty, A., Parida, K., "Enhanced photo catalytic reduction of Cr (VI) over polymer-sensitized g-C3N4/ZnFe2O4 and its synergism with phenol oxidation under visible light irradiation", *Catalysis Today,* 315 (2018) 52-66.
20. Thota, S., Kashyap, S. C., Sharma, S. K., Reddy, V. R., "Micro Raman, Mossbauer and magnetic studies of manganese substituted zinc ferrite nanoparticles: Role of Mn", *J. Phys. Chem. Solids,* 91 (2016) 136-144.
21. Rather, S., Lemine, O. M., "Effect of Al doping in Zinc ferrite nanoparticles and their structural and magnetic properties", *J. Alloys Compd*., 812 (2020).
22. Modaresi, N., Afzalzadeh, R., Aslibeiki, B., Kameli, P., Ghotbi-Varzaneh, A., Orue, I., Chernenko, V. A., "Magnetic properties of ZnxFe3-xO4 nanoparticles: a competition between the effects of size and Zn doping level", *J. Magn. Magn. Mater,* 482 (2019) 206-218.
23. Gul, S., Shahid, M., "Al-substituted zinc spinel ferrite nanoparticles: preparation and evaluation of structural, electrical, magnetic and photocatalytic properties", *Ceram. Int*., 46 (2020) 14195-14205.
24. Sobana, S., Alagumanian, S., Kumar, D., Sakthivel, P., Sivakumar, P., "Effect of Al3+incusion on characterization exploration, magnetic and anti-cancer properties of cobalt ferrite nanoparticles synthesized by co-precipitation process", *International Journal of Engineering and Advanced Technology*, (2020) 2249-2898.
25. Palange, S. M., Shrisath, S. E., Jangam, G. S., Lohar, K. S., Jadhav, S. S., "Relative structure refinement, cation distribution and magnetic Al^{+3} substituted $NiFe_2O_4$ nanoparticles", *AIP*, 109 (2011) 053909.
26. Waghmare, S. P., Borikar, D. M., Rewatkar, K. G., "Impact of Al doping on structure and magnetic properties of Co-ferrite", *Mater. Today. Proc*., 4 (2017) 11866-11872.
27. Shyamaldas, Bououdina, M., Manoharan, C., "Dependence of structure/morphology on electrical/magnetic properties of hydrothermally synthesized cobalt ferrite nanoparticles", *J. Magn. Magn. Mater*., 493 (2020) 165703.
28. Kumar-Das, K., Patnaik, S., Mansingh, S., Behera, A., Mohanty, A., Acharya, C., Parida, K. M., "Enhanced Photocatalytic Activities of Polypyrrole Sensitized Zinc Ferrite/Graphitic Carbon Nitride n-n Heterojunction towards Ciprofloxacin degradation, Hydrogen Evolution and Antibacterial Studies", *Journal of colloid and interface science,* 561 (2020) 551-567
29. Kumar-Das, K., Patnaik, S., Nanda, B., Chandra-Pradhan, A., Parida, K., "$ZnFe_2O_4$-Decorated Mesoporous Al_2O_3 Modified MCM-41: A Solar-Light-Active Photocatalyst for the Effective Removal of Phenol and Cr (VI) from Water", *Chemistry Select,* 4 (5) (2019) 1806-1819.
30. Ebrahimi, M., Raeisi-Shahraki, R., Seyyed-Ebrahimi, S. A., Masoudpanah, S. M., "Magnetic Properties of Zinc Ferrite Nanoparticles Synthesized by Coprecipitation Method", *J. Supercond. Nov. Magn*., 27(6) (2014) 1587-1592.
31. Amiri, M., Salavati-Niasari, M., Akbari, A., "Magnetic nanocarriers: Evolution of spinel ferrites for medical applications", *Adv. Colloid Interface Sci.,* 265 (2019) 29-44
32. Kefeni, K. K., Mamba, B. B., "Photocatalytic application of spinel ferrite nanoparticles and nanocomposites in wastewater treatment", Review, *Sustainable Materials and Technologies*, 23 (2020) e00140.

33. Zipare, K., Dhumal, J., Bandgar, S., Mathe, V., Shahane, G., "Superparamagnetic Manganese Ferrite Nanoparticles: Synthesis and Magnetic Properties", *Journal of Nanoscience and Nanoengineering*, 1(3) (2015) 178-182.
34. Marinca, F., Chicinaş, I., Isnard, O., "Structural and magnetic properties of the copper ferrite obtained by reactive milling and heat treatment", *Ceram. Int*., 39(4) (2013) 4179-4186.
35. Mozaffari, M., Masoudi, H., "Zinc Ferrite Nanoparticles: New Preparation Method and Magnetic Properties", *J. Supercond. and Nov. Magn*., 27(11) (2014) 2563-2567.
36. Atif, M., Hasanain, S. K., Nadeem, M., "Magnetization of sol-gel prepared zinc ferrite nanoparticles: Effects of inversion and particle size", *Solid State Commun*, 138(8) (2006) 416-421.
37. Thapa, D., Kulkarni, N., Mishra, S. N., Paulose, P. L., Ayyub, P., "Enhanced magnetization in cubic ferrimagnetic $CuFe_2O_4$ nanoparticles synthesized from a citrate precursor: The role of Fe^{2+}", *J. Phys. D Appl. Phys*., 43(19) (2010) 195004.
38. Li, F., Wang, H., Wang, L., Wang, J., "Magnetic properties of ZnFe2O4 nanoparticles produced by a low-temperature solid-state reaction method", *J. Magn. Magn. Mater*., 309(2) (2007) 295-299.
39. Phuruangrat, A., Kuntalue, B., Thongtem, S., Thongtem, T., "Synthesis of cubic CuFe2O4 nanoparticles by microwave hydrothermal method and their magnetic properties", *Mater. Lett*. 167(2016) 65-68.
40. Sathiyamurthy, K., Rajeevgandhi, C., Bharanidharan, S., Sugumar, P., Subashchandrabose, S., "Electrochemical and Magnetic Properties of Zinc Ferrite Nanoparticles through Chemical Co-Precipitation Method", *Chemical Data Collections* ,28(2020) 100477.
41. Roy, S., Ghose, J., "Mössbauer study of nanocrystalline cubic CuFe2O4 synthesized by precipitation in polymer matrix", J. *Magn. Magn. Mater*., 307(1) (2006) 32-37.
42. Kanagesan, S., Hashim, M., AB-Aziz, S., Ismail, I., Tamilselvan, S., Alitheen, N. B., Swamy, M. K., Purna-Chandra-Rao, B., "Evaluation of Antioxidant and Cytotoxicity Activities of Copper Ferrite (CuFe2O4) and Zinc Ferrite ($ZnFe_2O_4$) Nanoparticles Synthesized by Sol-Gel Self-Combustion Method", *Appl. Sci*., 6(9) (2016) 184.
43. Mulud, F. H., Dahham, N. A., Waheed, I. F., "Synthesis and Characterization of Copper Ferrite Nanoparticles", *IOP Conf. Ser.: Mater. Sci. Eng*., 928(7) (2020) 072125.
44. Thandapani, P., Ramalinga-Viswanathan, M. Denardin, J. C., "Magneto caloric Effect and Universal Curve Behavior in Super paramagnetic Zinc Ferrite Nanoparticles Synthesized via Microwave-Assisted Co-Precipitation Method", *Phys. Status Solidi B Basic Res*., 215(11) (2018) 1700842.
45. Kavitha, N., Manohar, P., "Magnetic and electrical properties of magnesium substituted Ni-Zn ferrites", *J. Supercond and. Nov. Magn.,* 29(8) (2016) 2151-2157.
46. Babu, B. R., Prasad, M. S. R., Ramesh, K. V., "Role of Synthesis on Physical Properties of Ni0.5Zn0.5Fe2 O4Nanoferrite: A Comparative Study", *J. Supercond. and Nov. Magn*., 30 (2017) 1609-1617.
47. Paramesh, D., Vijaya-Kumar, K., Venkat-Reddy, P., "Effect of aluminum substitution on the electrical properties of Ni-Zn nano ferrites", *J. Magn. Magn. Mater*., 444 (2017) 371–377.
48. Chand, P., Vaish, S., Kumar, P., "Structural, optical and dielectric properties of transition metal (MFe_2O_4; M = Co, Ni and Zn) nano ferrites", *Phys. B Condens. Matter*., 524 (2017) 53-63.
49. Chahar, D., Taneja, S., Thakur, P., Thakur, A., "Remarkable resistivity and improve dielectric properties of Co–Zn nano ferrites for high frequency applications", *J. Alloys Compd*., 843 (2020) 155681.
50. Anu, K., Hemalatha, J., "Magnetic and electrical conductivity studies of zinc doped cobalt ferrite nanofluids", J. Mol. Liq. 284 (2019) 445-453.
51. Rezaei, B., Kermanpur, A., Labbaf, S., "Effect of Mn addition on the structural and magnetic properties of Zn-ferrite nanoparticles", *J. Magn. Magn. Mater.*, 481 (2019) 16-24.
52. Rana, K., Thakur, P., Sharma, P., Tomar, M., Gupta, V., Thakur, A.," Improved structural and magnetic properties of cobalt nano ferrites: influence of sintering temperature", *Ceramics Int.,* 41 (2015) 4492-4497.
53. Mathur, P., Thakur, A., Lee, J. H., Singh, M., "Sustained electromagnetic properties of Ni-Zn-Co nano ferrites for the high-frequency applications", *Mater. Lett*, 64(24) (2010) 2738-2741.
54. Rameshbabu, R., Kumar, N., Karthigeyan, A., Neppolian, B., "Visible light photocatalytic activities of ZnFe2O4/ZnO nanoparticles for the degradation of organic pollutants", *Materials Chemistry and Physics*, 181 (2016) 106-115.
55. Yadollahpour, A., "Magnetic Nanoparticles in Medicine: A Review of Synthesis Methods and Important Characteristics", *Oriental Journal of Chemistry*, 31 (2015) 271-277.
56. Iqbal, A., Saeed, R., "Bio-Synthesis, Characterization and Catalytic Potential of Nanoparticles for Dyes Removal", *Int. J. Nanosci. and Nanotechnol*., 20(1) (2024)1-9.
57. Divya, B., Karthikeyan, C., Rajasimman, M., "Chemical Synthesis of Zinc Oxide Nanoparticles and Its Application of Dye Decolourization", *Int. J. Nanosci. and Nanotechnol*, 14(4) (2018) 267-275.
58. Aghagoli, M. J., Shemirani, F., "Hydrothermal Synthesis of Cobalt Disulfide Nanostructures and Adsorption Kinetics, Isotherms, and Thermodynamics of Tetracycline", *Int. J. Nanosci. and Nanotechnol.*, 15(4) (2019) 219-228.

59. Vanaja1, A., Suresh, M., Jeevanandam, J., “Facile Magnesium Doped Zinc Oxide Nanoparticle Fabrication and Characterization for Biological Benefits”, *Int. J. Nanosci. and Nanotechnol.*, 15(4) (2019) 277-286.
60. Mesvari, S., Shariaty-Niassar, M., Karimi-Sabet, J., Dastbaz, A., “Lithium Extraction by Metal Organic Framework-Based Adsorbent (MnO2@Co/ZnZIF) from Aqueous Solutions”, *Int. J. Nanosci. and Nanotechnol*., 20(2) (2024), 129-142.
61. Ghafouri-Taleghani, H., Soleimani-Lashkenari, M., Fazli, S., Ghorbani, M., “Polyaniline/Fe3O4/Poly (Methyl Methacrylate) Nanocomposites as an Acrylic Resin Coating for Enhancement of Anticorrosion Properties of Alkyd Paints”, *Int. J. Nanosci. and Nanotechnol.,* 17(4) (2021) 209-220.
62. Budi, S., “The Controllable Growth of CoNiCu Nanoalloy Electrodeposited from Electrolyte-Containing Alkyl Polyglucoside”, *Int. J. Nanosci.and Nanotechnol*., 20(2) (2024) 103-111.
63. Saravanan, S., Sivanandan , T., Ramalingam, G. “Optical, Thermal and Magnetic Properties of Strontium Ferrite Nanoparticles”., *Int. J. Nanosci. and Nanotechnol*., 18(4) (2022) 275-284.